

Bridging electrostatic properties between nanoscopic and microscopic highly charged droplets

Victor Kwan and Styliani Consta*

*Department of Chemistry, The University of Western Ontario, London, Ontario, Canada
N6A 5B7*

E-mail: sconstas@uwo.ca

Abstract

The chemical reaction mechanisms within electrosprayed droplets are still unknown. The location of ions provides insight into these mechanisms. We demonstrate the convergence of ion spatial distributions in aqueous droplets using molecular dynamics. This convergence allows one to extrapolate the simulation results from nanoscopic dimensions to larger ones, which are still inaccessible to atomistic modeling. The surface excess charge and electric field are also computed. We find that the surface excess charge layer is approximately 1.5 nm-1.7 nm thick and that $\approx 55\% - 33\%$ (from smaller to larger droplets) of the total number of ions reside in this layer.

Introduction

In the last one and a half decades there has been a surge in the use of nano- and micro-drops in many applications in science and industry. Examples include dispersive liquid-liquid micro-extraction,¹ micro- and nano-fluidity and acceleration of reactions in electrosprayed droplets.²⁻⁷ Even though our ability to carry out chemical reactions on mass-scale in these minute volumes is rapidly growing, the knowledge of the reaction mechanisms of the dissolved species in the droplet environment is still limited.

In this article, we consider charged droplets in aerosol phase for which we compute systematically the ion spatial distribution, surface excess charge, and electric field as a function of droplet size. To our knowledge this is the first study that addresses convergence of electrostatic properties of nano-droplets and finds the portion of ions (free charge) that contributes in the surface excess charge. Moreover, for the first time a molecular foundation on the equilibrium partitioning model of C. Enke^{8,9} is reported. In the computations, we use Na^+ and Cl^- ions in aqueous droplets to demonstrate the effects. Nevertheless, the findings and the methodologies are transferable to any other ions and solvents. Droplet sizes that are accessible to experimental scrutiny are atomistically modeled.

The study is directly relevant to several aerosol-based experiments and to atmospheric chemistry.¹⁰⁻¹² Such experiments include a recent development in the use of electrosprayed droplets as reaction vessels²⁻⁶ and droplet-based ionization techniques used in native mass spectrometry.¹³ Finding the ion distribution is the first step to establish the ion-evaporation mechanism (IEM),¹⁴⁻¹⁶ and the equilibrium partitioning model of C. Enke,^{8,9} which are broadly used to explain the selectivity effectiveness of electrospray ionization mass spectrometry (ESI-MS). IEM and Enke models have been inferred by the analysis of mass spectrometry

data. Our study provides the thus far missing knowledge of a droplet’s molecular structure.

A lot of experience has been obtained over many decades from the molecular modeling of related systems such that of ions near a planar interface^{17–21} and from the electrical double layer studies in electrochemistry and colloidal science.^{22,23} These systems are overall neutral, thus the findings may not be directly transferable to charged droplets.

Charged droplets are metastable states for which the competition between surface and electrostatic forces determines their survival time. In the analysis of the data we will use the Rayleigh limit for a conducting droplet,^{24–26} which we define in the following paragraph. The stability of a conducting charged droplet is determined by the dimensionless Rayleigh fissility parameter^{24–26} (X)

$$X = \frac{Q^2}{64\pi^2\gamma\epsilon_0 R^3} \approx \left(\frac{Q}{Q_r}\right)^2 \quad (1)$$

where Q is the droplet charge, γ the surface tension, ϵ_0 and R are the permittivity of vacuum and the radius of the droplet, respectively. For a certain radius R and a surface tension, one can find a value of charge, denoted by Q_r hereafter, such that $X = 1$. The $X = 1$ condition is called the Rayleigh limit.²⁴ A droplet may have a charge Q that may be different from Q_r . Thus, one can recast the Rayleigh fissility parameter by the ratio of charges squared as given in the second equality in Eq. 1. A droplet at $X < 1$ (below the Rayleigh limit) is separated from the fragmented state (progeny droplets) by a free energy barrier.^{14–16,27} The consensus view for droplet fragmentation is that a highly charged micro-drop at $X \approx 1$ reduces its charge by emitting a jet of smaller progeny charged droplets (comprised solvent and ions).²⁸ The jet release from the parent droplet is known as Rayleigh fission or Coulomb fission. It has been suggested that when the radius of nanodrops is ≈ 10 nm, the release of charge may take place before Rayleigh fission by emission of small clusters that contain solvated single ions.^{14,15} This is called the ion-evaporation mechanism (IEM). We think that the difference between a

Rayleigh fission mechanism and an IEM may be subtle when release of ion-clusters occurs slightly below the Rayleigh limit in nanodrops. In this article we discuss the structure of an intact droplet and we draw relations with the IEM and Enke model.

Systems and Simulation Methods

We performed equilibrium molecular dynamics (MD) simulations of charged aqueous droplets with Na^+ , Cl^- ions. A typical snapshot of a system comprised H_2O molecules, Cl^- and Na^+ ions is shown in Fig. 1. Table 1 shows the systems that have been studied and their characteristics. The simulations were performed by using the software NAMD version 2.12.²⁹ The Newton’s equation of motion for each atomic site was integrated using the velocity-Verlet algorithm with a time step of 1.0 fs. The trajectories were analyzed using VMD 1.9.2.³⁰ The water molecules were modeled with the TIP3P (transferable intermolecular potential with 3 points)³¹ -CHARMM and the ions with the CHARMM36m^{32,33}

All the forces were computed directly without any cut-offs. Equilibrium simulations in NAMD were set by placing the droplet in a spherical cavity of radius 20.0 nm by using spherical boundary condition. The cavity was sufficiently large to accommodate the shape fluctuation of the droplet. The droplet will eventually reach vapor pressure equilibrium. The systems were thermalized with Langevin thermostat with the damping coefficient set to 1/ps. In the estimation of the Rayleigh limit the surface tension value for TIP3P at $T = 300$ K is taken to be 0.0523 N/m and at $T = 350$ K 0.0432 N/m³⁴ for a planar interface. The analysis of the droplet electric field and potential is done with in-house methodology and software, of which details are presented in the article of Kwan et al.³⁵

The production runs of the 2×10^4 and 3×10^4 H_2O -molecule drops were for 40 ns, following a 10 ns equilibration time and that of 1000 and 3500 H_2O -molecule clusters for 150 ns and 50 ns, respectively. The production run for the

Table 1: Systems studied, characteristic dimensions and concentrations. $n_{\text{H}_2\text{O}}$ denotes average number of water molecules and n_{I} number of ions in the droplets during the production runs. R_e [nm] is the equimolecular radius, computed by using density of the TIP3P model at 350 K to be 0.9539 g/cm³. Q_r (e) is the charge estimated at the Rayleigh limit using radius R_e . r_{max} [nm] is the distance from the droplet center of mass (COM) to the maximum of the ion concentration profile. R_r [nm] is the Rayleigh radius ($X = 1$) for charge equal n_{I} . X is the fissility parameter of the simulated droplet (Eq. 1). “Range” [nm] denotes the interval defined from the droplet COM in which the surface excess charge is located. Details are presented in the text. C [Molarity] is the ion concentration in the region of the excess charge. In all the systems the temperature is set at $T = 350$ K, besides those marked with an asterisk, which are found at $T = 300$ K.

$n_{\text{H}_2\text{O}}$	n_{I}	R_e	Q_r	R_r	r_{max}	X	Range	n_{out}	C [M]
880	6Na ⁺	1.88	7.9	1.56	0.90-0.95	0.57	1.2±0.1-2.6	3.3±0.6	0.08 ±0.03
5880	19Na ⁺	3.65	20.6	3.37	2.65-2.70	0.85	2.6±0.1-4.4	10.6±1.2	0.06 ±0.02
2×10^4	36Na ⁺	5.31	37.6	5.16	4.30-4.35	0.92	4.4±0.1-6.1	13.5±1.3	0.04 ±0.01
3×10^4	44Na ⁺	6.08	46.0	5.90	5.10-5.15	0.91	5.2±0.1-6.8	14.7±2.1	0.03 ±0.01
3×10^4	44Na ⁺ + 23 NaCl	6.08	46.0	5.90	5.10-5.15	0.91	5.2±0.1-6.8	18.2±2.1	0.04 ±0.01
6×10^4	63Na ⁺	7.66	65.1	7.50	6.90-6.95	0.94	6.9±0.1-8.3	15.3±2.3	0.03 ±0.01
880	6Cl ⁻	1.88	7.9	1.56	1.05-1.10	0.57	1.2±0.1-2.6	3.7 ±0.6	0.09 ±0.03
980*	8Cl ⁻	1.92	8.2	1.92	1.15-1.20	0.95	1.3±0.1-2.8	3.7 ±0.6	0.07 ±0.03
3×10^4	44Cl ⁻	6.08	46.0	5.90	5.10-5.15	0.91	5.2±0.1-6.8	14.7±2.1	0.03 ±0.01
3×10^4	44Cl ⁻ + 23 NaCl	6.08	46.0	5.90	5.10-5.15	0.91	5.2±0.1-6.8	16.5±2.1	0.04 ±0.01

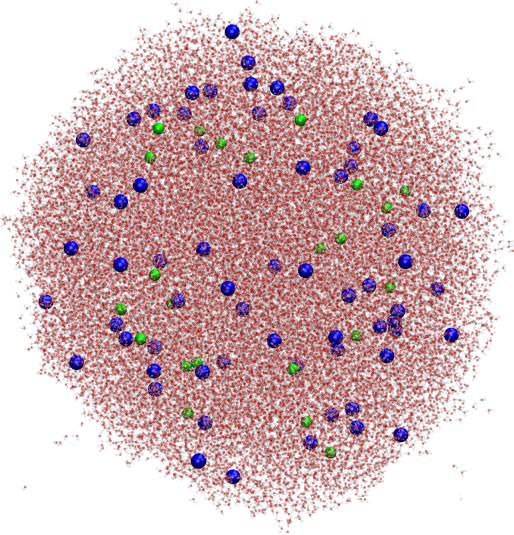


Figure 1: Typical snapshot of a droplet that comprises $\approx 3 \times 10^4$ TIP3P molecules (red oxygen site, white hydrogen site) and 23 Cl^- ions (green spheres) and 67 Na^+ ions (blue spheres).

6×10^4 H_2O -molecule drop was 8.5 ns.

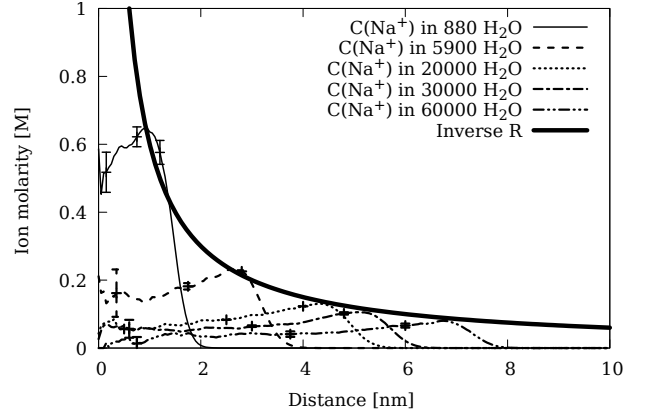
Results and Discussion

Convergence of ion spatial distributions

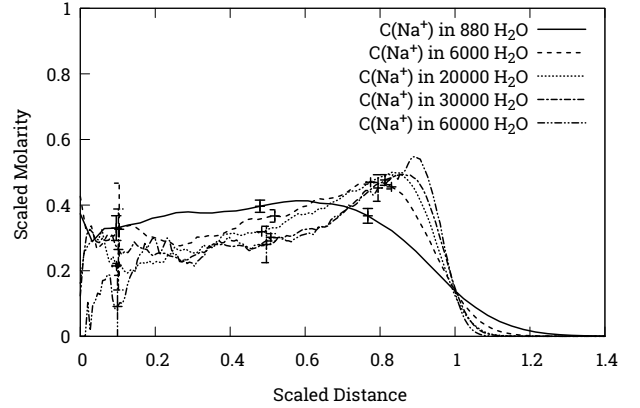
Below, we attempt to rationalize universal features of the charge density distribution in a droplet close to the Rayleigh limit. In Figure 2 (a) we show the ion distributions for five droplet sizes shown in Table 1 (see also Fig. S1 in SI). The profiles have been normalized by dividing the raw histogram data with the volume element of a spherical shell ($\frac{4}{3}\pi[(r+dr)^3 - r^3]$ where r is the distance from the droplet COM). We can recast Eq. 1 into the following form

$$\frac{1}{(4\pi\epsilon_0)^2} \frac{Q^2}{R^4} R = |E|^2 R = 4\epsilon_0\gamma X \quad (2)$$

where $|E| = Q/4\pi\epsilon_0 R^2$ is the magnitude of the electric field on the surface of a spherical conductor with radius R (we remind that in this model all the charge lies on the surface and there are no shape fluctuations). Eq. 2 shows that the surface charge density, denoted here-



(a)



(b)

Figure 2: (a) Na^+ concentration profiles vs distance from the droplet COM for aqueous droplets of various sizes at $T = 350$ K. Standard deviation bars are sparsely shown for clarity purpose. The standard deviation is shown in Fig. 3. (b) Scaled plots of (a). The x-axis is scaled by R_r for the specific droplet charge state (Q) and the y-axis by Q/R_r^3 (data presented in Table 1).

after by $\sigma = \epsilon_0|E|$.³⁶ Hence, Eq. 2 becomes

$$\sigma^2 = \frac{4\gamma X}{\epsilon_0} \quad (3)$$

On the other hand, the surface charge density is computed by integrating the ion molarity $n(x)$ from the surface of the droplet to the droplet center

$$\sigma = \frac{1}{4\pi R^2} \int_0^\infty dr 4\pi r^2 n(r) \quad (4)$$

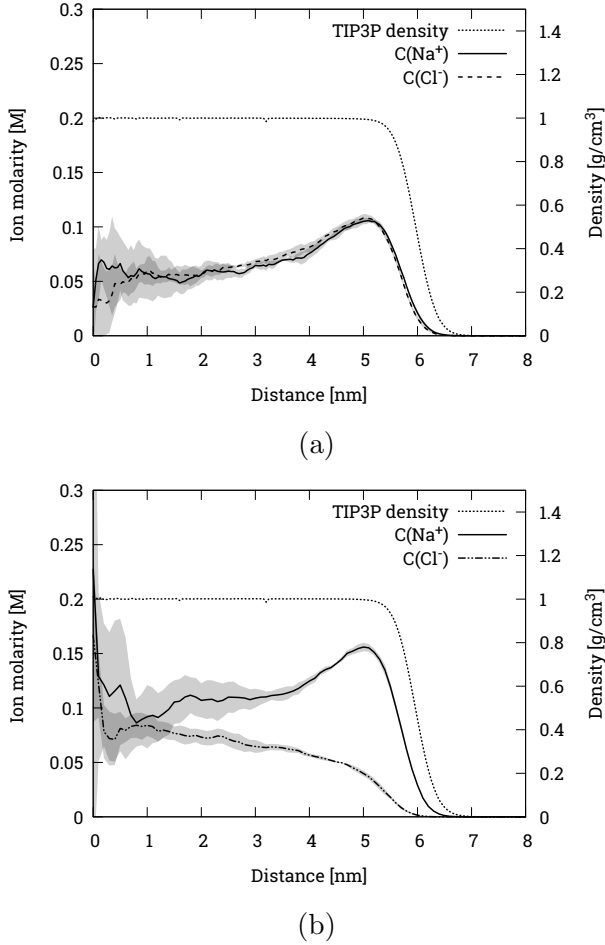


Figure 3: Same as Fig.2 (a) but (a) for a droplet comprised $\approx 3 \times 10^4$ H_2O molecules and either 44 Na^+ ions or 44 Cl^- ions. (b) $\approx 3 \times 10^4$ H_2O molecules, 44 Na^+ ions and 23 NaCl pairs. The blurry region shows the standard deviation. The standard deviation is calculated by using 5 blocks of raw data, where every block has 4×10^4 configurations, separated by 0.2 ps.

where the charge density is computed in units of $[\text{mol}]/[\text{m}]^2$. We note that $n(r)$ is given by the non-linear Poisson-Boltzmann (PB) equation. $n(r)$ drops sharply on the surface because of lack of shape fluctuations and decays towards the droplet COM. If the charge is localized near the surface of a droplet we may approximate the surface by a planar interface. The solution of the nonlinear PB equation relates the charge molarity on the surface of the droplet $n(R)$ and the surface charge density (for details see³⁵)

$$\sigma = \lambda_{PB} n(R) \quad (5)$$

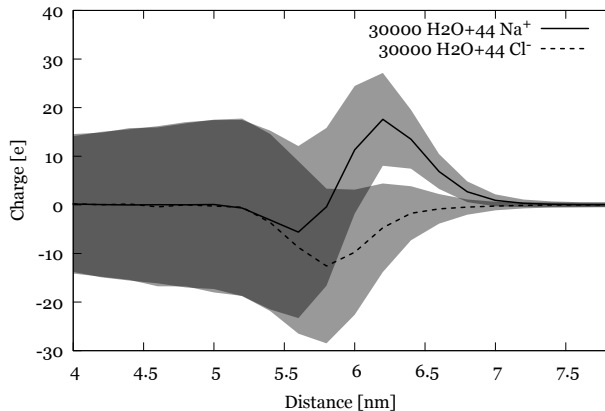
where λ_{PB} is a parameter emerging from the solution of the non-linear PB equation, that remarkably coincides with the Debye length of electrolyte with the ion molar concentration $n(R)$. The “Debye length” scales as $\lambda_{PB} \sim 1/\sqrt{n(r)}$, therefore, after some algebra we arrive at the relation for the surface charge density derived from the solution of the non-linear PB equation $\sigma^2 \sim n(R)$. Combining this result with Eq. 2 we arrive at the scaling for the maximum ionic concentration as a function of the droplet radius $n(R) \sim X/R$. The simulation data agree with the theoretical prediction (Eq. 2) that the surface charge density σ decreases with the increase of the droplet radius as shown in Fig. 2 (a). Figure 2 (b) shows the scaled distributions, where the distance (x axis) in Fig. 2 (a) has been scaled by R_r shown in Table 1. The scaled distributions reveal an interesting behavior that it is not evident in the non-scaled data (Figure 2 (a)). The distributions of all droplet sizes apart from that of 880 H_2O molecules are very similar.

In the largest droplets comprising 6×10^4 H_2O molecules the scaled ion density decays faster than all the rest. The diminished magnitude of the relative shape fluctuations results in a sharper maximum of the ion density distribution. The larger relative shape fluctuations of the smallest droplets give rise to three features in the ion concentration profile. Firstly, the concentration profile of 880 H_2O molecules-6 Na^+ ions appears to be much broader than those for the larger droplets. Secondly, the distance of r_{max} from the droplet very outer surface where the water density is $5 \times 10^{-4} \text{ g/cm}^3$ becomes shorter as the droplet size increases. This distance is $\approx 1.7 \text{ nm}$ for the smallest droplet and $\approx 1.4 \text{ nm}$ for the largest droplet. $|R_e - r_{max}|$ follows the same trend: it is $\approx 1.0 \text{ nm}$ for the smallest droplet and $\approx 0.74 \text{ nm}$ for the largest droplet. In microscopic droplets the distance of the maximum of the ion distribution to R_e (see Table 1) may become even shorter because of the reduced relative shape fluctuations. We estimated that the ratio of r_{max}/R_r changes from 0.59 for droplets of 880 H_2O molecules to 0.92 for droplets of 6×10^4 H_2O molecules. The ratio of r_{max}/R_r vs R_r is

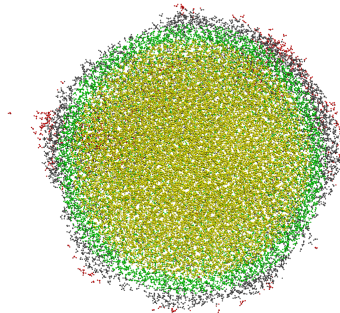
shown in Fig. S2 in SI, where extrapolation of the data led to the intriguing observation that $r_{max}/R_r = 1$ when $R_r \approx 10$ nm. At this point we relate our finding to IEM.^{14,15} The observation suggests that certain fluctuations in charge density (or shape since shape and charge density are intimately related) in droplets with radius less than 10 nm may be responsible for a faster release of solvated ions via IEM^{14,15} than a Rayleigh fission mechanism. The role of fluctuations has not been considered in the original formulation of IEM.^{14,15} The specifics of Rayleigh fluctuations vs fluctuations underlying the IEM mechanism deserve a separate study.

Counterions are commonly found in solutions. We examine the role of counterions and contrast it with systems without counterions. Figure 3 (a) shows the spatial ion distribution of droplets comprised $\approx 3 \times 10^4$ H₂O molecules, and either 44 Na⁺ ions or 44 Cl⁻ ions. The r_{max} of the Cl⁻ ions is slightly more in the interior relative to the Na⁺ ions. Figure 3 (b) shows the ion distribution of a droplet comprised $\approx 3 \times 10^4$ H₂O molecules, 44 Na⁺ ions and 23 NaCl pairs. A main feature in Fig. 3 is that in a droplet with counterions the excess ions (Na⁺) form an outer shell of higher concentration. The Cl⁻ ions are depleted from the region where the Na⁺ concentration is the highest and their concentration gradually increases toward the droplet center. The location of the Cl⁻ ions is the result of the conducting character of the droplet, which dictates that the excess charge accumulates on the surface. If we scale the Na⁺ concentration in the presence of Cl⁻ ions the two concentrations with and without counterions coincide. In the presence of counterions, the Na⁺ concentration (not scaled) appear to extend more toward the outer H₂O layers and to have higher concentration in the interior. This behavior is attributed to the fact that in the presence of counterions the concentration of Na⁺ is higher in order to maintain the overall charge of the droplet the same as that without counterions. This increased outer concentration indicates that the surface is not saturated with free charge when only Na⁺ ions are present.

Surface excess charge and electric field



(a)



(b)

Figure 4: (a) Charge distribution of a droplet (including H, O, ions comprised 3×10^4 H₂O molecules and either 44 Na⁺ ions or 44 Cl⁻ ions vs distance from the droplet COM (bin size 2.0 Å). (b) Colored shells centered at the droplet COM: yellow colored $0 \text{ \AA} < r < 50.0 \text{ \AA}$, green colored $50.0 \text{ \AA} < r < 56.0 \text{ \AA}$, grey colored $56.0 \text{ \AA} < r < 62.0 \text{ \AA}$, red colored $r > 62.0 \text{ \AA}$.

A relevant quantity to that of the ion spatial distribution is that of the surface excess charge. Figure 4 (a) shows the charge distribution of a droplet comprised 3×10^4 H₂O molecules and either 44 Na⁺ ions or 44 Cl⁻ vs distance from the droplet COM (see also Fig. S3 and Fig. S4 in SI for the polarization charge and cumulative charge distribution, respectively). The onset of the building up of the charge is found at $\approx 5.1 \pm 0.1$ nm, which is in the green colored region shown in Fig. 4 (b). At ≈ 5.1 nm the ion concentration is at its maximum value. For Na⁺ ions the charge distribution profile un-

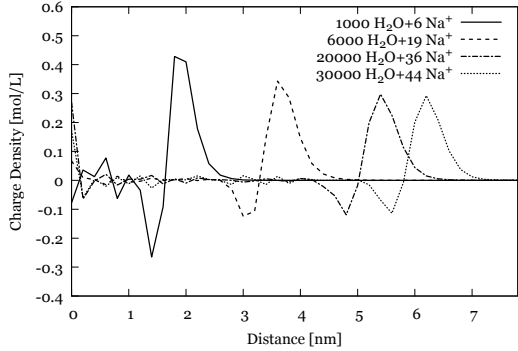


Figure 5: Charge density (sum of Na^+ , oxygen, hydrogen sites), in aqueous droplets with Na^+ ions as a function of droplet size.

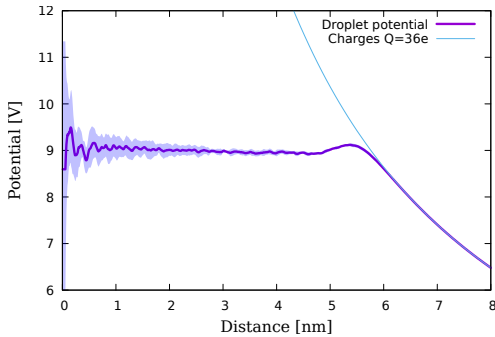


Figure 6: Average radial potential of a droplet comprising 2×10^4 H_2O molecules and 36 Na^+ ions. Contribution from all the point charges (H , O , Na^+) is considered.

ulates at distance > 5.1 nm. The integral from 5.1 nm outward yields the total charge of the droplet ($43e$ - $44e$). In Table 1 we have reported the range over which the integration is performed. The upper limit of integration is at the distance where the water density becomes $5 \times 10^{-4} \text{ g/cm}^3$. In our simulations and in experimental set-ups a droplet may be surrounded by vapor. As we have shown in previous work³⁵ this vapor is also polarized. Thus, the presence of the vapor may extend the surface charge but its contribution is insignificant. As shown in Table 1 the smallest droplet contributes $\approx 55\%$ of the free charge in the surface charge, while the largest droplets $\approx 37 - 33\%$. The errors bars in the number of ions in the surface excess charge region is due to the uncertainty in the initial point of the interval over which the integration is performed. The error bars associated with the ion distribution and

water density in this region is negligible because both have converged. The concentration of ions in the surface excess charge layer is also shown in Table 1. We remind here that the ion distribution is not uniform in the range of the excess surface charge (see Fig. 2). We note that the charge undulation is not unique to the positively charged droplets, but it also appears in an uncharged water droplet^{37,38} (see Fig. S5 in SI). In the presence of Na^+ ions the charge undulation in pristine and positively charged droplet are in-phase but the building-up of the charge starts at a shorter distance relative to the uncharged case. The positive peak relative to that of the pristine water is higher because of the stronger orientation of the outer water molecules with the hydrogen sites pointing outwards. These water molecules are mainly found in the grey- and red-colored region of Fig. 4 (b). The Cl^- show only one negative trough in the charge distribution (Fig. 4 (a)), which is much broader than the negative trough of the Na^+ ions. The Cl^- ions themselves enhance the negative trough of the pristine water molecules. The positive peak of the pristine water disappears because of the change in the orientation of the water molecules due to the overall negative charge of the droplet. Figure 5 shows the progression in the normalized charge distribution profiles as a function of droplet size for positive ions. The charge undulation becomes less pronounced with increased droplet size due to the decrease of the ion concentration as the droplet size increases.

In a previous work, Ahadi et al.³⁹ have placed the surface charge in charged droplets in the very outer periphery (water/vapor interface) of the droplet, where the density of water is reduced substantially and does not include any free charge. It appears that Ahadi et al.³⁹ attempt to define the droplet surface charge in the region where the total charge comprises only solvent polarization (no ions). We relate now the findings of Ahadi et al.³⁹ with our plots. Figure 4 shows that for the droplet of 44 Na^+ ions, the integral of the charge from 6.18 nm (top of the positive peak) outwards, yields charge very close to $+44e$. We have found the same for all the positively charged droplets

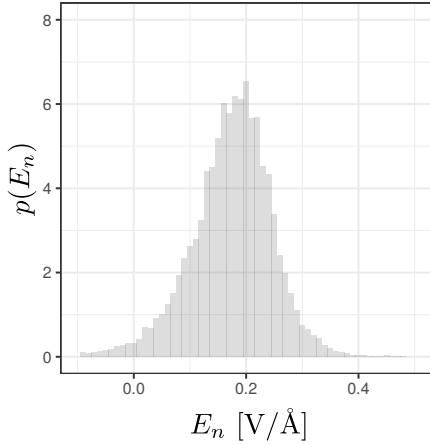
shown in Fig. 5. This interval of integration corresponds to the red region in Fig. 4 (b) where there are no ions, thus this region appears to be close to Ahadi et al. assignment of the surface charge. Here we point out differences between assigning the surface charge in the very outer region vs the thick layer shown in Fig. 4. Firstly, since the outer positive peak for positive ions (Fig. 4 (a)) is very steep, the values of the charge in the outer droplet region is very sensitive to the starting point of integration. Secondly, because of the similarity of the charge undulation between pristine water droplets and positively charged droplets, the existence of positive charge (= total droplet charge) in the farthest water layers is not surprising. Differently, in the presence of Cl^- ions we cannot find an interval over which the integral yields the overall droplet charge located in the very outer water layers. For the Cl^- ions we have to integrate over the range reported in Table 1. Thus, it not evident that for both positive and negative ions we can find the total charge in the form of polarization charge in the farthest water layers. Thirdly, the physical and chemical significance of the surface charge in the red region of Fig. 4 (b) is not well defined because the outer “inert” solvent molecules cannot explain the mass spectrometry abundances. It is the presence of active species (ions and possibly other species) that play a critical role in abundances. We emphasize here that the size of the standard deviation indicates that there are large charge fluctuations in the outer droplet layers, which may lead to release of solvated single ions or charge transfer processes to macroions (when macroions are present). The standard deviations in the definition of the droplet radius and charge density have not been considered in the article by Ahadi et al.,³⁹ hence the significant sensitivity of the periphery surface charge on the definition of the droplet radius has not been discussed.

Figure 6 shows the electrostatic potential of a droplet comprising 2×10^4 H_2O molecules and 36 Na^+ ions. For large distance the potential coincides with that of a point charge with $Q = 36e$. Inside the droplet the potential can be well approximated by a constant value

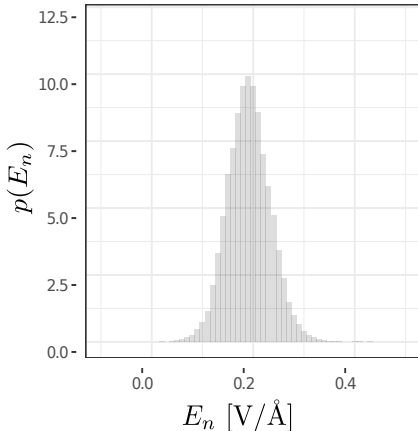
(within the error bars), which is the potential on the surface of the droplet. The potential raises in a region of 4.8 nm - 5.8 nm. This region starts from the minimum of the negative trough of the charge distribution (Fig. 5) and ends beyond the positive peak. The starting point of integration that yields the total droplet charge is the outer region is found approximately in the middle of the “hump”. The starting point of integration at 5.9 nm where the dielectric and conducting behavior differentiate, yields a charge ($+4e$) which is much less than the overall droplet charge.

At this point it is in order to relate our findings with the equilibrium partitioning model of C. Enke. The model relates the analyte response using ESI-MS to the location of the analytes in a droplet.^{8,9} The Enke model assumes similarity between the structure of a charged droplet and the electric double layer found on the surface of an electrode in contact with a solution. In the case of a droplet, the role of the electrode is assumed by the vacuo (or air). Thus, the model identifies two regions in a droplet. The outer region which is the excess charge region and an inner core region. Electrolyte and analyte ions partition between these two regions by establishing an equilibrium. The model infers that the species seen in the mass spectrum are those that make up the surface charge. The foundation of the model is in agreement with the simulation findings presented here.

Now, we examine the electric field on the droplet surface. The shape fluctuations prevent a direct computation of the electrostatic potential and electric field on the droplet surface because of the large statistical errors.^{35,40} We have developed an approach (details are presented in Ref.³⁵) to reconstruct the droplet surface and then compute the electric potential by using a multipole expansion. The normal component of the electric field for a droplet comprised 2×10^4 H_2O molecules and 36 Na^+ ions is shown in Fig. 7 (a) and that of the same droplet size and charge, but with all the charge on a single ion is shown in Fig. 7 (b). The electric field is computed for this specific droplet size over all its surface and over a number of con-



(a)



(b)

Figure 7: (a) Distribution of the normal component of the electric field on the molecular surface of a droplet comprised 2×10^4 H₂O molecules and 36 Na⁺ ions. (b) Same as (a) but the charge is all accumulated on a single ion.

figures. The average electric field on the surface is 0.187 [V/Å] for both charge distributions, however in the conducting droplet (a), on 2% of the total area of the droplets used in the analysis the electric field magnitude is twice the average value but in the droplet (b) the fluctuations of the field are much smaller. This difference may be expected because in droplet (b) the charge is not transferred on the surface, thus the surface charge is close to that of pure water. The electric potential throughout a droplet with a united charge is shown in Fig. S5 (b) in SI. Comparison with the findings by Kwan et al.³⁵ for a conducting droplet of

1000 H₂O molecules - 8 Na⁺ ions shows that the droplet electric field in the larger droplet decreases. This is expected since the larger the droplet, the lower the ion concentration. Moreover, the fluctuations of the electric field on the droplet surface decrease, which may explain the dominance of IEM in charged droplets with radius ≈ 10 nm.¹⁴⁻¹⁶ The average value of the electric field is in agreement with range of values reported in experiments.^{41,42} Our computations also show the magnitude of the fluctuations, which cannot be readily estimated in experiments.

Conclusions

The new insights we obtained from this study are: (a) The maximum ionic concentration scaling is $n(R) \sim 1/R$, which allows us to infer the location of the maxima in larger droplets than those that can be simulated thus far. For droplets that range in size between several hundreds to several tens of thousands of water molecules $|R_e - r_{max}|$ changes from approximately 1.0 nm for the smallest droplet to 0.74 nm for the largest droplet. (b) Scaling of the x-axis of the ion distributions by the Rayleigh radius of the droplet, reveals that for droplets with diameter, 7 nm (which is $\approx 6 \times 10^3$ H₂O molecules) to 16 nm the ion distribution profiles almost coincide. For the droplet of diameter 5 nm (≈ 1000 H₂O molecules) the Na⁺ scaled concentration profile is broader than the other sizes. The profile for the smallest droplet is determined by the relative large shape fluctuations. (c) The presence of counterions plays a dramatic role in the manner in which the ions are distributed. The ions in excess are situated in the exterior while the counterions reside in the droplet interior. (d) We found that the surface excess charge comprises of $\approx 55\% - 33\%$ (decreasing from the smaller to the larger droplets) of the total number of ions and the solvent polarization charge. The thickness of the layer with the surface excess charge is 1.5 nm-1.7 nm. This thickness appears invariant in all the droplet sizes we have studied. The amount of free charge in the surface

excess charge region decreases with increasing droplet radius and converges with increasing droplet radius. Our findings are in agreement with the foundation of the equilibrium partitioning model of C. Enke.^{8,9} Computations of the droplet surface electric field show the magnitude of its fluctuations. We think that these fluctuations underlie the ion-evaporation mechanism. (e) Finally, our analysis indicates that at droplet radius ≈ 10 nm the difference in values between r_{max} , R_r and R_e becomes negligible. Interestingly, this limit coincides with the droplet radius below which the ion evaporation mechanism dominates over the Rayleigh fission for droplet disintegration. We think that this coincidence is not fortuitous and requires further investigation of the droplet shape fluctuations.

Supplementary Material

See supplementary material of (a) cumulative distribution profiles; (b) Surface excess charge data.

Acknowledgement S.C. is grateful to Prof. D. Frenkel, Department of Chemistry, University of Cambridge, UK, Prof. S. S. Xantheas, Pacific Northwest National Laboratory and Dr. Anatoly Malevanets, The University of Western Ontario for discussions on the stability of charged systems. S.C. acknowledges an NSERC-Discovery grant (Canada) for funding this research. Sci-Net, SHARCNET and Compute Canada are acknowledged for providing the computing facilities.

References

- (1) Rezaee, M.; Assadi, Y.; Hosseini, M.-R. M.; Aghaee, E.; Ahmadi, F.; Berijani, S. Determination of organic compounds in water using dispersive liquid-liquid microextraction. *J. Chromatogr. A* **2006**, *1116*, 1–9.
- (2) Chen, X.; Cooks, R. G. Accelerated reactions in field desorption mass spectrometry. *J. Mass Spectrom.* **2018**, *53*, 942–946.
- (3) Schrader, R. L.; Fedick, P. W.; Mehari, T. F.; Cooks, R. G. Accelerated Chemical Synthesis: Three Ways of Performing the Katritzky Transamination Reaction. *J. Chem. Educ.* **2019**,
- (4) Lee, J. K.; Banerjee, S.; Nam, H. G.; Zare, R. N. Acceleration of reaction in charged microdroplets. *Q. Rev. Biophys.* **2015**, *48*, 437–444.
- (5) Ingram, A. J.; Boeser, C. L.; Zare, R. N. Going beyond electrospray: mass spectrometric studies of chemical reactions in and on liquids. *Chem. Sci.* **2016**, *7*, 39–55.
- (6) Sahraeian, T.; Kulyk, D. S.; Badu-Tawiah, A. K. Droplet Imbibition Enables Non-Equilibrium Interfacial Reactions in Charged Microdroplets. *Langmuir* **2019**,
- (7) Consta, S.; Kapral, R. Dynamics of proton transfer in mesoscopic clusters. *J. Chem. Phys.* **1996**, *104*, 4581–4590.
- (8) Enke, C. G. A predictive model for matrix and analyte effects in electrospray ionization of singly-charged ionic analytes. *Analytical Chemistry* **1997**, *69*, 4885–4893.
- (9) Constantopoulos, T. L.; Jackson, G. S.; Enke, C. G. Effects of salt concentration on analyte response using electrospray ionization mass spectrometry. *Journal of the American Society for Mass Spectrometry* **1999**, *10*, 625–634.
- (10) Mather, T.; Harrison, R. Electrification of volcanic plumes. *Surv. Geophys.* **2006**, *27*, 387–432.
- (11) Nelson, J.; Baker, M. Charging of ice-vapor interfaces: applications to thunderstorms. *Atmos. Chem. Phys.* **2003**, *3*, 1237–1252.
- (12) Pähz, T.; Herrmann, H. J.; Shinbrot, T. Why do particle clouds generate electric charges? *Nature Physics* **2010**, *6*, 364.
- (13) Wilm, M. Principles of electrospray ionization. *Mol. Cell. Proteomics* **2011**, *10*, M111–009407.

- (14) Iribarne, J. V.; Thomson, B. A. On the evaporation of small ions from charged droplets. *J. Chem. Phys.* **1976**, *64*, 2287–2294.
- (15) Thomson, B.; Iribarne, J. Field induced ion evaporation from liquid surfaces at atmospheric pressure. *J. Chem. Phys.* **1979**, *71*, 4451–4463.
- (16) Consta, S.; Mainer, K. R.; Novak, W. Fragmentation mechanisms of aqueous clusters charged with ions. *J. Chem. Phys.* **2003**, *119*, 10125–10132.
- (17) Jungwirth, P.; Tobias, D. J. Specific ion effects at the air/water interface. *Chem. Rev.* **2006**, *106*, 1259–1281.
- (18) Dang, L. X.; Schenter, G. K. Rate theory of ion pairing at the water liquid–vapor interface: A case of sodium iodide. *J. Chem. Phys.* **2018**, *148*, 222820.
- (19) Nguyen, M.; Rick, S. W. The influence of polarizability and charge transfer on specific ion effects in the dynamics of aqueous salt solutions. *J. Chem. Phys.* **2018**, *148*, 222803.
- (20) Smith, J.; Rick, S. W. Ion clustering in aqueous salt solutions near the liquid/vapor interface. *arXiv preprint arXiv:1603.07106* **2016**,
- (21) Petersen, P. B.; Saykally, R. J. On the nature of ions at the liquid water surface. *Annu. Rev. Phys. Chem.* **2006**, *57*, 333–364.
- (22) Stillinger Jr, F. H.; Kirkwood, J. G. Theory of the diffuse double layer. *The Journal of Chemical Physics* **1960**, *33*, 1282–1290.
- (23) Dukhin, S.; Derjaguin, B. *Electrokinetic Phenomena*; J. Willey and Sons, 1974.
- (24) Rayleigh, L. XX. On the equilibrium of liquid conducting masses charged with electricity. *Philos. Mag.* **1882**, *14*, 184–186.
- (25) Hendricks, C.; Schneider, J. Stability of a conducting droplet under the influence of surface tension and electrostatic forces. *Am. J. Phys.* **1963**, *31*, 450–453.
- (26) Oh, M. I.; Malevanets, A.; Paliy, M.; Frenkel, D.; Consta, S. When droplets become stars: charged dielectric droplets beyond the Rayleigh limit. *Soft Matter* **2017**, *13*, 8781–8795.
- (27) Consta, S.; Malevanets, A. Disintegration mechanisms of charged nanodroplets: novel systems for applying methods of activated processes. *Mol. Simul.* **2015**, *41*, 73–85.
- (28) Grimm, R. L.; Beauchamp, J. Evaporation and discharge dynamics of highly charged multicomponent droplets generated by electrospray ionization. *J. Phys. Chem. A* **2009**, *114*, 1411–1419.
- (29) Phillips, J. C.; Braun, R.; Wang, W.; Gumbart, J.; Tajkhorshid, E.; Villa, E.; Chipot, C.; Skeel, R. D.; Kalé, L.; Schulten, K. Scalable molecular dynamics with NAMD. *J. Comput. Chem.* **2005**, *26*, 1781–1802.
- (30) Humphrey, W.; Dalke, A.; Schulten, K. VMD: Visual Molecular Dynamics. *J. Mol. Graphics* **1996**, *14*, 33–38.
- (31) Jorgensen, W. L.; Jenson, C. Temperature dependence of TIP3P, SPC, and TIP4P water from NPT Monte Carlo simulations: Seeking temperatures of maximum density. *J. Comput. Chem.* **1998**, *19*, 1179–1186.
- (32) Noskov, S. Y.; Roux, B. Control of Ion Selectivity in LeuT: Two Na⁺ Binding Sites with Two Different Mechanisms. *J. Mol. Biol.* **2008**, *377*, 804 – 818.
- (33) Beglov, D.; Roux, B. Finite representation of an infinite bulk system: Solvent boundary potential for computer simulations. *J. Chem. Phys.* **1994**, *100*, 9050–9063.

- (34) Vega, C.; de Miguel, E. Surface tension of the most popular models of water by using the test-area simulation method. *J. Chem. Phys.* **2007**, *126*, 154707.
- (35) Kwan, V.; Malevanets, A.; Consta, S. Where do the ions reside in a highly charged droplet? *J. Phys. Chem. A* **2019**, *123*, 9298–9310, PMID: 31589448.
- (36) Jackson, J. D. *Classical Electrodynamics*, third ed. ed.; John Wiley & Sons: New York, NY, 1998.
- (37) Zakharov, V. V.; Brodskaya, E. N.; Laaksonen, A. Surface tension of water droplets: A molecular dynamics study of model and size dependencies. *J. Chem. Phys.* **1997**, *107*, 10675–10683.
- (38) Zakharov, V. V.; Brodskaya, E. N.; Laaksonen, A. Surface properties of water clusters: a molecular dynamics study. *Mol. Phys.* **1998**, *95*, 203–209.
- (39) Ahadi, E.; Konermann, L. Surface charge of electrosprayed water nanodroplets: A molecular dynamics study. *J. Am. Chem. Soc.* **2010**, *132*, 11270–11277.
- (40) Beck, T. L. The influence of water interfacial potentials on ion hydration in bulk water and near interfaces. *Chem. Phys. Lett.* **2013**, *561*, 1–13.
- (41) Hogan Jr, C. J.; Carroll, J. A.; Rohrs, H. W.; Biswas, P.; Gross, M. L. Combined charged residue-field emission model of macromolecular electrospray ionization. *Anal. Chem.* **2009**, *81*, 369–377.
- (42) Beroz, J.; Hart, A.; Bush, J. W. Stability limit of electrified droplets. *Phys. Rev. Lett.* **2019**, *122*, 244501.